Langmuir

Article

pubs.acs.org/Langmuir

Effect of Counterions on the Shape, Hydration, and Degree of Order at the Interface of Cationic Micelles: The Triflate Case

Filipe S. Lima,[†] Iolanda M. Cuccovia,[†] Dominik Horinek,[‡] Lia Q. Amaral,[∥] Karin A. Riske,[⊥] Shirley Schreier,[†] Roberto K. Salinas,[†] Erick L. Bastos,[†] Paulo A. R. Pires,[†] José Carlos Bozelli, Jr.,[†] Denize C. Favaro,[†] Ana Clara B. Rodrigues,[#] Luís Gustavo Dias,[§] Omar A. El Seoud,[†] and Hernan Chaimovich*[,†]

[†]Instituto de Química and [∥]Instituto de Física, Universidade de São Paulo, São Paulo, Brazil

[‡]Institut für Physikalische und Theoretische Chemie, Universität Regensburg, Regensburg, Germany

[⊥]Departamento de Biofísica, Universidade Federal de São Paulo, São Paulo, Brazil

[#]Centro de Ciências Naturais e Humanas, Universidade Federal do ABC, Santo André, Brazil

[§]Departamento de Química, FFCLRP, Universidade de São Paulo, Ribeirão Preto, Brazil

Supporting Information

ABSTRACT: Specific ion effects in surfactant solutions affect the properties of micelles. Dodecyltrimethylammonium chloride (DTAC), bromide (DTAB), and methanesulfonate (DTAMs) micelles are typically spherical, but some organic anions can induce shape or phase transitions in DTA^+ micelles. Above a defined concentration, sodium triflate (NaTf) induces a phase separation in dodecyltrimethylammonium triflate (DTATf) micelles, a phenomenon rarely observed in cationic micelles. This unexpected behavior of the DTATf/NaTf system suggests that DTATf aggregates have unusual properties. The structural properties of DTATf micelles were analyzed by time-resolved fluorescence quenching, small-angle X-ray scattering, nuclear magnetic resonance, and electron paramagnetic resonance and compared with those of DTAC, DTAB, and DTAMs micelles. Compared to the other micelle types, the DTATf micelles had a higher average number of monomers per aggregate, an uncommon disk-like shape, smaller interfacial hydration, and restricted monomer chain mobility. Molecular dynamic simulations supported these observations. Even small water-soluble salts can profoundly affect micellar properties; our data demonstrate that the $-CF_3$ group in Tf^- was directly responsible for the observed shape changes by decreasing interfacial hydration and increasing the degree of order of the surfactant chains in the DTATf micelles.

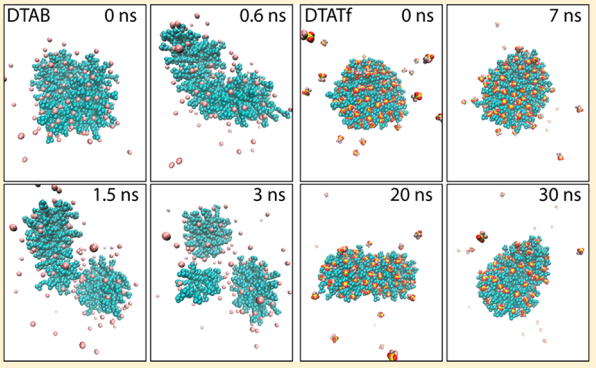

INTRODUCTION

The properties of ionic micelles can be affected by salt,[1,2] surfactant concentration,[3,4] and temperature.[5,6] In particular, the ion adsorption at the micellar interface controls the ionization degree (α), critical micelle concentration (cmc), Kraft temperature, aggregation number (N_{agg}), and phase/shape transitions.[7−13] Several models of counterion binding to micelles partially describe the interactions between charged counterions and monomer headgroups.[14−22] The hydrophobic interactions between the micellar core and the hydrophobic moiety of the organic counterions also affect micellar stability. Theoretical models have included these interactions.[23] Large organic counterions can penetrate into the micellar core to some extent, inducing micellar growth.[24−27] Ionic dehydration upon counterion binding[28,29] and ion-pair formation,[29−32] parameters that should be incorporated in a full description of counterion binding, have only been included in a few models.[33,34] At the present level of theory, it is difficult to predict the properties of ionic micelles with soluble counterions that are relatively small and dehydrated and possess the ability to form ion pairs. An increased understanding of the effects of counterions on the packing of monomers into aggregates would be beneficial.

Sodium triflate (NaTf) produces a greater decrease in the surface tension of water than any other simple salt.[13,35] At 318 K, the α of dodecyltrimethylammonium (DTA^+) triflate (Tf^-) micelles (DTATf) is three to five times smaller than that of aggregates formed by the same surfactant with bromide (Br^-) (DTAB)[36] or chloride (Cl^-) (DTAC)[37] as the counterion, respectively. The unusually high Kraft temperature of DTATf was attributed to an ion pair formation, similar to the formation observed in cationic micelles with large counterions.[38] The low

Received: November 22, 2012
Revised: January 31, 2013
Published: March 8, 2013

   dx.doi.org/10.1021/la304658e | Langmuir 2013, 29, 4193−4203

hydration of the $-CF_3$ moiety[39] of Tf^- may play a central role in its binding to DTA micelles. In micelles, Tf^- may have a preferential orientation comparable to that proposed for the same counterion in ionic liquids.[40] The rotation of water molecules surrounding DTATf micelles is less affected by the presence of the aggregates than in other DTA-based surfactants, suggesting that a more dehydrated micelle is produced when triflate is used as the counterion.[41]

Here, we demonstrate that the properties of DTATf micelles are unusual, with high aggregation numbers at low surfactant concentrations. The low degree of counterion dissociation suggested a favorable interaction between the headgroups and the counterion, and low hydration at the micelle interface. In contrast to the spherical or rod-like structures typically observed in micelle structures, the DTATf aggregate had a bicelle-like structure, possibly with interdigitated hydrophobic chains. This micellar shape was the result of highly packed monomers in the aggregate, which reduced DTA^+ mobility inside the hydrophobic core and prevented water penetration. Molecular dynamics simulations supported high affinity binding of the triflate to DTA^+ to generate DTATf aggregates with increased stability.

MATERIALS AND METHODS

Materials. Trifluoromethanesulfonic acid (triflic acid), DTAB, pyrene (Py), and NaOH were from Sigma-Aldrich (St. Louis, MO, USA, Analytical grade). Water was deionized and bidistilled. Dodecylpyridinium chloride (Aldrich) was recrystallized in a methanol/acetone mixture. Deuterium oxide (D_2O) from Aldrich was bidistilled. The 4-(*N*,*N*-dimethyl-*N*-hexadecyl)ammonium-2,2,6,6-tetramethylpiperidine-1-oxyl iodide (CAT16) was from Molecular Probes. The 4-hydroxy-2,2,6,6-tetramethylpiperidinil-1-oxyl (Tempol) and 5-doxyl stearic acid methyl ester (5MESL) were from Sigma. All other reactants and solvents were analytical grade or better and used without further purification.

Dodecyltrimethylammonium triflate and sodium triflate (DTATf and NaTf, respectively) were prepared as previously described.[13] Dodecyltrimethylammonium methanesulfonate (DTAMs) and chloride (DTAC) were prepared by passing a methanolic solution of DTAB (5 g in 30 mL methanol for each surfactant) through an ion-exchange resin column (Purolite, Purolite, SGA550OH, OH^- form) previously saturated with sodium methanesulfonate or chloride, respectively. The methanol was removed by rotoevaporation, and the surfactants were recrystallized in methanol/ether.

Methods. *Time Resolved Fluorescence Quenching, TRFQ.* An aliquot of a stock ethanolic Py solution was added to the aqueous surfactant solution. The [Py] and [micelles] ratios were maintained below 0.025 to prevent excimer formation. Dodecylpyridinium chloride was added to a final concentration of (up to) 2 quencher molecules per micelle. Experiments were performed in an Edinburgh FLS920 fluorescence spectrometer system with Time Correlated Single Photon Counting (318.0 ± 0.5 K). The lifetime fluorescence decay kinetics were recorded with λ_{EX} = 335.6 nm and λ_{EM} = 383.6 nm with a window of 1 μs with 2048 channels. N_{agg} was calculated, based on the Infelta[42]–Tachiya[43] model, from an analysis of the characteristic time decay of fluorescence intensity of micellized Py as a function of the [Py] (eq 1):[44]

$$I(t) = I_0 \cdot \exp\left\{-\frac{t}{\tau_0} + \frac{N_{agg} \cdot [q]}{c - \mathrm{cmc}}[\exp(-k_q \cdot t) - 1]\right\} \quad (1)$$

where $I(t)$, I_0, τ_0, [q], c, and k_q are the fluorescence intensity at time t, the fluorescence intensity at time zero, the probe fluorescence lifetime in absence of quencher, the quencher concentration, the surfactant concentration, and the second-order quenching rate constant, respectively. The routine used for the analysis of the TRFQ curves is available in the Supporting Information. For each surfactant concentration, the fluorescence decay kinetics of pyrene was recorded with five different quencher concentrations in duplicate. For a given [DTATf], an apparent aggregation number, N'_{agg}, was calculated for each [Py]. The N_{agg} value for a specific surfactant concentration was taken as the average over the N'_{agg} computed for this [DTATf], and the error of N_{agg} is the standard deviation of the average.

Small Angle X-ray Scattering (SAXS). SAXS measurements were obtained with a NanoStar small-angle X-ray instrument (Bruker AXS) with Cu $K\alpha 1$ radiation λ = 1.54 Å. The sample-to-detector distance was 679 mm. The scattering data were collected by a two-dimensional position-sensitive gas detector (HiSTAR) with the scattering vector, $q = 4\pi \sin \theta/\lambda$, ranging from 0.014 $Å^{-1}$ to 0.35 $Å^{-1}$, using 2θ as the scattering angle. The samples were conditioned in 2-mm inner diameter quartz capillaries. The temperature was controlled by a water circulating bath. The SAXS curves were corrected for solvent scatter and sample attenuation. Experiments were performed at 328 K and room temperature.

The SAXS curves were fitted with the program GENFIT[45,46] using two minimization routines (SIMANN and SIMPLEX). Only the form factor was taken into account during the fitting procedure. For all tested geometries, the aggregate structure was assumed to consist of two density levels, representing the hydrated headgroup (shell) and the hydrocarbon chain (core) regions. The parameters for the bicelle rim were assumed to be the same as those for the bilayer part. Because all the curves exhibited a similar peak profile, the curve obtained with the highest [DTATf] was chosen for the fitting procedure. All fits were performed assuming $\rho_{solvent}$ = 0.33 e/Å with no background correction.

Nuclear Magnetic Resonance, NMR. All spectra were recorded with a Bruker 500 MHz Avance III spectrometer at 318 K. Dried surfactants were weighed in volumetric flasks to obtain the desired surfactant concentration, followed by the addition of 0.6 M NaTf from a D_2O stock solution. The volumes were completed with D_2O and transferred to 5 mm NMR tubes. All samples were pre-equilibrated for 10 min before measurements. The ^1H longitudinal magnetization relaxation times (T_1) were measured by the inversion–recovery experiment. The ^1H transverse magnetization relaxation times (T_2) were measured by a Carr-Purcell-Meiboom-Gill pulse sequence experiment. Both pulse sequences programs were provided by Bruker. The 2D (^1H–^1H) NOE spectra were recorded with different mixing times (τ_{mix}) varying from 0.2 to 1 s (0.3 M DTAB) or 0.1 to 1 s (0.1 M DTATf).

The following procedure was used to calculate the NMR order parameter (S). For processes dominated by dipole–dipole interactions, such as those in micellar systems, T_1 and T_2 are defined by the following relations:[47]

$$\frac{1}{T_1} = A[J(\omega) + 4J(2\omega)] \quad (2)$$

$$\frac{1}{T_2} = \frac{A}{2}[3J(0) + 5J(\omega) + 2J(2\omega)] \quad (3)$$

$$A = \left[\frac{3(n-1)}{20}\right]\left[\frac{\mu_0 \gamma_H^2 h}{8\pi^2 r_{H-H}^3}\right]^2 \quad (4)$$

The parameter $J(\omega)$ is the spectral density, and the variables n, μ_0, γ_H, h, and r_{H-H} represent the number of geminal protons, the permeability of the vacuum, the proton gyromagnetic ratio, Planck's constant, and the distance between the geminal protons, respectively. Using an assumption of two correlation times, Wennerström et al.[48] have developed a two-step model for the analysis of NMR relaxation data. Using a picosecond time scale, one correlation time, τ_f, is related to the fast motion of the monomers. On a nanosecond time scale, the other correlation time, τ_s, corresponds to the overall tumbling of the aggregate. Assuming that τ_f is in the extreme narrowing limit and the micelle tumbling is isotropic, the relationship between the spectral density function and the two correlations times can be written as follows:[49]

dx.doi.org/10.1021/la304658e | *Langmuir* 2013, 29, 4193–4203

$$J(\omega) = S^2\left(\frac{2\tau_s}{1 + (\omega_0\tau_s)^2}\right) + (1 - S^2)2\tau_f \quad (5)$$

where S is the NMR order parameter of the H−H internuclear vector and ω_0 is the ^{1}H spin Larmor frequency. An expression for S as a function of T_1, T_2, and τ_s can be obtained by subtracting eq 2 from eq 3 and combining the result with eq 5:[50]

$$S^2 = \frac{1}{3A}\left(\frac{1}{T_2} - \frac{1}{T_1}\right)\left(\tau_s + \frac{\tau_s}{1 + (\omega_0\tau_s)^2} - \frac{2\tau_s}{1 + (2\omega_0\tau_s)^2}\right)^{-1} \quad (6)$$

The slow correlation time (τ_s) can be calculated from the Stokes−Einstein equation for (pure) DTAB. For the DTATf aggregates, τ_s was calculated according to a model of noncharged disk-like particle motion in water, which depends only upon the geometric parameters of the particles.[51]

Electron Paramagnetic Resonance, EPR. EPR spectra were obtained in a Bruker EMX-200 spectrometer (T = 318.0 ± 0.5 K). Samples were added to flat quartz cells and measured at a frequency of approximately 9.4 GHz, with a sweep width of 100 G, a modulation amplitude of 1.0 G, and a time constant of 0.163 s. Spectra were analyzed with WINEPR software (Bruker). Two spin probes, CAT16 and 5MESL (Chart 1). The concentration of spin label stock solutions

Chart 1. Structure of CAT16 (top) and 5MESL (bottom)

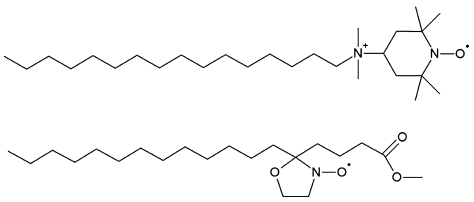

in chloroform were determined by EPR using Tempol as a standard.[52] Stock solutions of the micelles with the desired concentration were prepared in water by weighing the proper mass of the salts. The incorporation of the spin label into the micelles was made as briefly described. A spin label film was produced in glass vials, after evaporation under N_2 of spin label stock solutions. The spin label films were then put under vacuum for at least 2 h to ensure complete elimination of the solvent. Micelle solutions of the desired concentration were used to suspend the spin label films. The vials were left for at least 30 min under ultrasonic bath at 323 K before use. The final molar ratio of spin label and micelles was approximately 1 in all cases.

Rotational correlation times (τ_B and τ_C) of the two probes, CAT16 and 5MESL, were calculated from spectral line heights and line widths using Kivelson[53] and Freed and Fraenkel[54] theories. The equations for τ_B and τ_C are (eqs 7 and 8):[55]

$$\tau_B = -1.27 \times 10^{-9}\frac{W_0}{2}\left[\left(\sqrt{\frac{h_0}{h_{+1}}}\right) - \left(\sqrt{\frac{h_0}{h_{-1}}}\right)\right] \quad (7)$$

$$\tau_C = -1.19 \times 10^{-9}\frac{W_0}{2}\left[\left(\sqrt{\frac{h_0}{h_{+1}}}\right) - \left(\sqrt{\frac{h_0}{h_{-1}}}\right) - 2\right] \quad (8)$$

where W_0 is the peak-to-peak width of the central line and h_0, h_{+1}, and h_{-1} are the height of central, low, and high field line, respectively. The geometric mean of τ_B and τ_C provide an effective rotational correlation time ($\tau_{measured}$), as reported in micellar systems.[56] The value of $\tau_{measured}$ incorporates the micellar tumbling time (τ_S) and the time for the reorientation of the probe relative to the micelle (τ_{probe}). In a spherical aggregate, these rotational correlation times are assumed to be independent:[57]

$$\frac{1}{\tau_{measured}} = \frac{1}{\tau_S} + \frac{1}{\tau_{probe}} \quad (9)$$

Using the same model of DTATf tumbling as described above,[51] we assumed that the separation of both relaxations for a disk-like particle can be treated as described by eq 9.

Molecular Dynamics Simulations. The simulations were performed within a cubic box with a 120 Å edge and consisting of 130 chains of DTA^+ (united atom) and 130 molecules of triflate or bromide. The initial DTATf aggregate was built with the Packmol software package[58] with the DTA^+ molecules in a bilayer arrangement, with the edges exposed to water and the counterions surrounding the aggregate, at ca. 4 Å from the N atom at the DTA headgroups. The box was filled with approximately 55 000 SPC/E water molecules. The force field used for the monomer was OPLS.[59] The force field used for the triflate was that described previously,[60] and the bromide parameters were also from the literature.[61] The DTA^+ charge was equally distributed among the four carbons directly bonded to N, which is neutral.[62,63] We used the geometric rule for all Lennard-Jones interactions. The simulations were performed at 318 K with a V-scale thermostat and a pressure of 1 bar maintained by an isotropic pressure coupling. Periodic boundary conditions were applied, and the Coulomb forces were calculated with the particle-mesh Ewald summation. Cutoff radii of 15 Å and 12 Å were used for the Coulomb interactions and the Lennard-Jones interactions, respectively, with a switch at 11.0 Å. The simulations were performed for 35 and 10 ns for DTATf and DTAB, respectively, with the GROMACS 4.5.5 software package[64] in double precision.

The extension of the triflate solvation shell around the DTA^+ micelle was determined from the distribution function (PDF) of the Tf^- center of mass (COM) distance, d, to the proximal atom of the DTA aggregate. Additional information was obtained from the residence time of Tf^- in a thin window along the proximal distance coordinate. Windows were defined so that the distance of the center of mass (COM) of the Tf^- to the nearest atom of the DTA aggregate was within a lower bound, r_{ll}, and an upper bound, r_{ul}. The window thickness was chosen as 0.3 Å. The coarse-grained residence function $f(t)$ of a given triflate was defined as f = 1 if the Tf^- was within the window, otherwise, f = 0. The residence time within this window was determined as the integral over the normalized autocorrelation function of $f(t)$ averaged over all counterions.

RESULTS AND DISCUSSION

Aggregation Number. TRFQ. N_{agg} of DTATf was determined using time-resolved fluorescence quenching (Figure 1). Values of τ_0 were in good agreement with the reported values for DTAB (not shown).[65] N_{agg} increased linearly with [DTATf] (Figure 1). The reported N_{agg} for 0.05 and 0.1 M DTAMs is 43.[41] The decay curves are available in the Supporting Information (Figure 1).

Increasing [DTAB] in aqueous solution from the cmc to 1 M increases N_{agg} from 66 to 83.[66] N_{agg} for DTAB also increases with salt concentrations up to 1 M NaBr. Above 2 M, a further steep increase in N_{agg} has been associated with a sphere-to-rod transition.[67] N_{agg} decreases moderately with temperature for both DTAB[68,69] and DTAC.[68] N_{agg} values of DTAC vary slightly with [DTAC] or [NaCl].[70−73] Despite the differences in absolute values, which are ascribable to diverse measuring techniques, under similar conditions, N_{agg} of DTAB micelles is higher than N_{agg} of DTAC. The values of N_{agg} of aqueous solutions of DTAB or DTAC at concentrations up to 0.1 M are always less than 71 (0.1 M DTAB at 283 K[56]). N_{agg} of DTAB at 4.0 M NaBr is 186,[67] and N_{agg} of DTAC at 2.5 M NaCl is 101[73] monomers per aggregate.

For micelles in 0.02 M DTATf, N_{agg} was 113, a value that was more than 1.5 times the highest value observed for pure DTAB or DTAC, even at low temperatures.[56] An additional increase in

dx.doi.org/10.1021/la304658e | Langmuir 2013, 29, 4193−4203

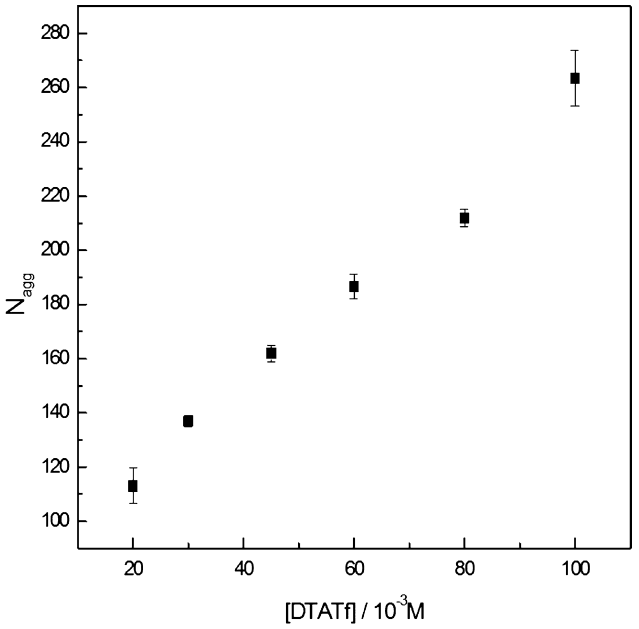

Figure 1. N_{agg} calculated from TRFQ as a function of [DTATf].

[DTATf] led to a further increase in N_{agg}, reaching 263 monomers per aggregate for [DTATf] = 0.1 M. The N_{agg} values obtained for DTAMs were closer to the values obtained for DTAC rather than DTATf, demonstrating the importance of the $-CF_3$ group in the triflate anion. The N_{agg} of dodecyltrimethylammonium perfluoroacetate (DTAPFA) is approximately 70 at 313 K,[74] and thus the CF_3 group by itself could not lead to high values of the aggregation number and the counterion binding.

The magnitudes of the N_{agg} determined here suggest that the DTATf aggregates cannot form spherical micelles. Considering the volume occupied by the hydrophobic chain and the radius of a sphere,[15] the maximum aggregation number for a spherical aggregate of a twelve carbon surfactant is approximately 55 monomers/micelle. This value is very close to the average value obtained for DTAC[70−73] (57 ± 9) and smaller than the values determined for DTAB[56,66−69,75] (69 ± 12), suggesting that the DTAC micelles are spherical and that the DTAB[66] and DTAPFA micelles[74] are quasi-spherical. DTAB and/or sodium dodecyl sulfate (SDS) have been proposed to form disk-like particles in D_2O solutions.[75,76] The monomers in DTAMs (N_{agg} = 43[41]) can also be confined into a spherical aggregate.

Micellar Shape. SAXS. The scattering curve obtained with 0.1 M DTATf at room temperature, where some crystals were present, exhibited a narrow peak at q = 0.267 Å^{-1}, arising from DTATf crystals with a cell parameter of 23.5 Å, a value that is consistent with the size of one molecule (Figure 3, Supporting Information). SAXS curves of 0.03, 0.08, and 0.1 M DTATf solutions at 328 K showed a broad band centered at q_1 = 0.20 Å^{-1}, with a narrow peak around q^* = 0.03 Å^{-1} and the q^* value was a function of [DTATf] (Figure 3, Supporting Information). A correlation distance, d^*, was estimated using the Bragg equation ($d^* = 2\pi/q^*$) for comparison with the mean distance between the aggregates ($\langle d\rangle$, $\langle d\rangle = ([(c - \mathrm{cmc})\cdot N_A]/(N_{agg}\cdot 10^{27}))^{-1/3}$), calculated with N_{agg} from TRFQ (Table 1). This interference peak at approximately 0.03 Å^{-1}, which resulted from the particle interactions, changed slightly with [DTATf] (Table 1). The d^* values from the SAXS experiments were in very good agreement with $\langle d\rangle$. The width of the

Table 1. Mean Distance between the Aggregates, $\langle d\rangle$, Calculated from N_{agg} Obtained from TRFQ, the Correlation Peak, q^*, and the Correlation Distance, d^*, Estimated from $2\pi/q^*$

[DTATf]/10^{-3} M	$\langle d\rangle$/Å[a]	q^*/Å^{-1}	d^*/Å[b]
30	208 ± 2	0.028	222 ± 48
80	167 ± 1	0.032	196 ± 42
100	166 ± 4	0.034	184 ± 39

[a]Error based on uncertainties in N_{agg} values. [b]Error estimated to be 20% in q^*.

interference peak indicated a short correlation length, most likely among first neighbors only. The maintenance of this correlation at even the lowest [DTATf] resulted from the low ionic strength of the solutions.

The intensity of the SAXS curve is given by $I = c\cdot P(q)\cdot S(q)$, where c is a constant, $P(q)$ is the object form factor, which is related to the electron density contrast of the object with the solvent, and $S(q)$ is the interference function, which accounts for the scattering interference among the objects. Taking into account only the form factor (i.e., $S(q) = 1$), the fits were performed using a starting value of q_{min} = 0.04 Å^{-1} to avoid the correlation peak at q^* approximately at 0.03 Å^{-1}. This choice of q_{min} was justified by the fact that the SAXS curves for DTATf in the presence of NaTf, which abolishes the interference among objects, were very similar to the curves for q > 0.04 Å^{-1} in the absence of salt (Figure 4, Supporting Information).

Micellar systems studied by SAXS exhibited a broad peak in $P(q)$ because of the interference in scattering between the two polar heads along the chain direction. This broad peak position at $q_1 \sim 0.2$ Å^{-1} is roughly connected with the distance between the centers of the two polar heads, and therefore gives a rough estimation of the thickness d_1 of the micellar structure, so that $d_1 \sim 2\pi/q_1 \sim 31$ Å. The SAXS curve is very sensitive to the symmetry of the micellar object, because $P(q)$ is decomposed in a factor related to the symmetry and a factor arising from the electron density profile along the chain direction. In the case of spherical symmetry, the sphere diameter is connected with the position q_1, but for cylindrical and planar symmetries q_1 is connected with, respectively, the cylinder diameter and the plane thickness, without information on the size of the micellar object. Therefore only for finite model it is meaningful to consider polydispersity in the finite size.

Different geometries were tested, including spherical, cylindrical, and ellipsoidal micelles, as well as an infinite bilayer and a finite bicelle with rims (Figure 2). The parameters of the different geometries are shown below (Table 2). For cylindrical micelles a model of finite cylinders was used, but the cylinder length was so large that it can be considered infinite. The size of the bicelle represents the disk diameter, and R_{shell} and R_{core} represent the thicknesses of the polar shell and the hydrophobic core, respectively (Chart 2). The bicelle was allowed to exhibit polydispersion, indicated by the error in Table 2.

Amphiphiles with one chain typically self-assemble into micelles, which can be spherical, cylindrical, or ellipsoidal. DTATf does not self-assemble into any of these micellar structures. These geometries were tested, but none resulted in a good fit (Figure 2) with reasonable parameters, as summarized in Table 2. The fits with the spherical micelle model produced a significantly narrower peak than the experimental curve. The overall peak shape was similar to the curve generated with the cylindrical model, but the behavior of the experimental curve at

dx.doi.org/10.1021/la304658e | Langmuir 2013, 29, 4193−4203

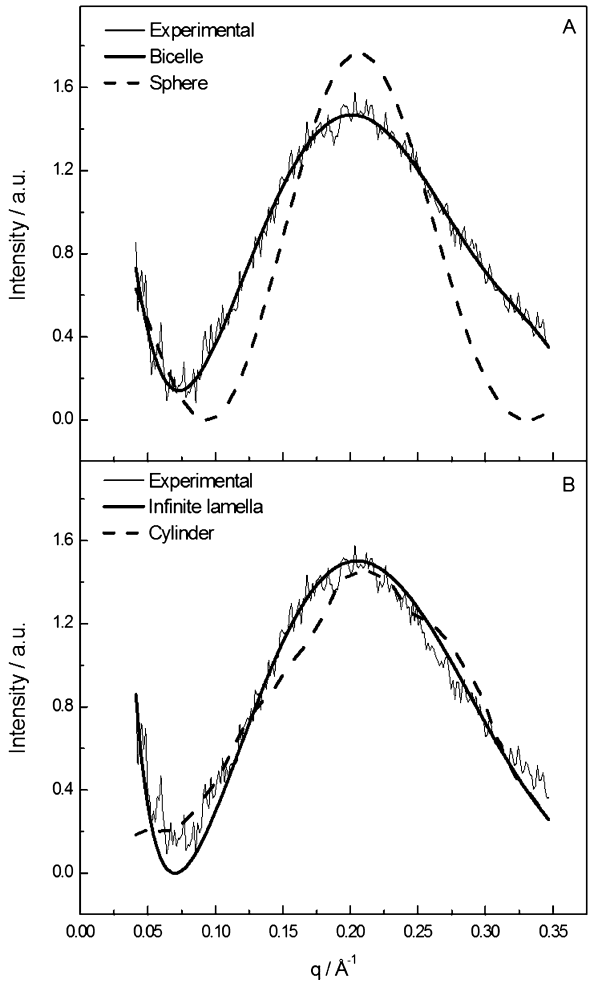

Figure 2. SAXS curve obtained with 0.1 M DTATf in water at 328 K. Four fits using different models are shown. The best fit parameters are given in Table 2.

Table 2. Parameters Used to Fit the Experimental Data with the Different Geometrical Models for the Form Factor of the 0.1 M DTATf Aggregates in Figure 2

model	R_{shell}/Å	R_{core}/Å	ρ_{shell}/e/Å^3	ρ_{core}/e/Å^3	size$_d$/Å
bicelle	6.0	9.2	0.43	0.30	54 ± 20
infinite lamella	6.0	8.0	0.40	0.29	∞
spherical micelle	4.0	15.8	0.40	0.28	-
cylindrical micelle	9.9	8.6	0.43	0.29	756

Chart 2. Structure Parameters of the Finite Bicelle Model

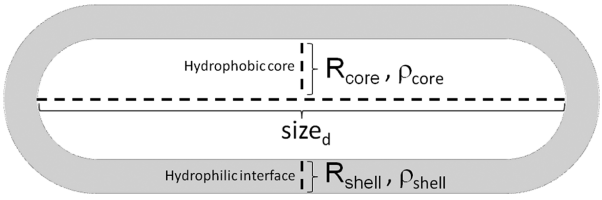

low q was definitely not achieved with the cylindrical geometry. The ellipsoidal micelle models were discarded (not shown). The oblate ellipsoid model did not generate a reasonable fit. The prolate ellipsoid model could reasonably fit the experimental curve but with very high anisometry between the two semiaxes, around 4, a value inconsistent with the accommodation of the surfactant molecules into this type of shape. A theoretical limit of anisometry of 1.8 for prolate micelles was previously determined. Values exceeding this limit suggest a spherocylinder conformation.[77]

The other tested geometry was a planar bilayer. Initially, a simple model with an infinite lamella was used. Surprisingly, this model resulted in a rather good fit (Figure 2) with realistic parameters (Table 2). The size of the hydrocarbon chain region was much smaller than the expected value of 16.7 Å for DTATf in a conventional bilayer in the fully extended configuration.[15] This observation suggested a high degree of interdigitation between the DTA^+ chains.

A refined bicelle model (with finite size) was used to fit the experimental curve with excellent results (Figure 2). The bilayer size parameters, shown in Table 2, were similar to those obtained with the simple infinite lamella model. These results suggest that the basic structure observed by X-ray was a bilayer with both size and rim effects contributing to a lesser extent to the curve profile. Unusual in ionic micellar systems, disk-like objects have been suggested by SANS experiments for cationic and/or anionic surfactant systems in D_2O solutions[75,76] and observed by microscopy.[11] Using a theory based on molecular thermodynamics, disk-like aggregates of fluorocarbon surfactants have been reported to be stable structures.[78] The *total* thickness of the hydrophobic DTATf core, i.e., $2R_{core}$, was 18.4 Å, a value that was only slightly higher than the predicted value of 16.7 Å for an *all trans* 12-carbon chain, suggesting an interdigitation of the DTA chains.[15] The predicted radius value of 16.7 Å is not realistic because not *all* hydrophobic chains of the monomers in the micelles would be fully extended at the same time. This value is smaller but very close to the minor axis obtained for DTAB aggregates.[66]

Local Order, Dynamics, and Hydration in DTAX Micelles. NMR. NMR methods are appropriate to determine the structural aspects of the micellar core without using probes.[79−82] The ^{1}H NMR spectra of DTATf, DTAMs, and DTAB in the presence of NaTf were assigned based on a comparison with the ^{1}D ^{1}H spectra of DTAC.[83]

The measured ^{1}H NMR chemical shifts of DTAB were consistent with the reported values for DTAC.[83] The addition of NaTf to the DTAB solutions of different [NaTf]/[DTAB] molar ratios ($R_{[NaTf]/[DTAB]}$) led to chemical shift displacements and line broadening that was more evident in the H1 proton and unresolved ($-CH_2-$) regions (HG) (Figure 3). The HG protons were split into two peaks in the DTAB solution, with only one observed peak in pure DTATf (Figure 3). This effect was similar to that reported for the addition of salicylate to DTAB, a system which undergoes a sphere-to-rod transition at a defined Br^-/salicylate ratio.[84] The observed line broadening resulted from a combination of tight chain packing with a long tumbling time of the aggregates as a function of [Tf^-].

The fundamental role of the $-CF_3$ group in the triflate with regard to the properties reported here and in the literature[13] became apparent from the values of the calculated order parameters (Table 3), S, from T_1 and T_2 (the values of relaxation times are shown in Table 1, Supporting Information). We used the two-step model[48] to calculate a NMR order parameter (S) for the protons at different positions in the DTA^+ chains (see the Methods section). The calculations yielded different values of S for HP, HG, and H12. The S value for the HP protons in DTATf was 5−6 times larger than those observed in DTAB or DTAMs. This large increase must arise from a highly packed interface in DTATf relative to DTAB or

dx.doi.org/10.1021/la304658e | *Langmuir* 2013, 29, 4193−4203

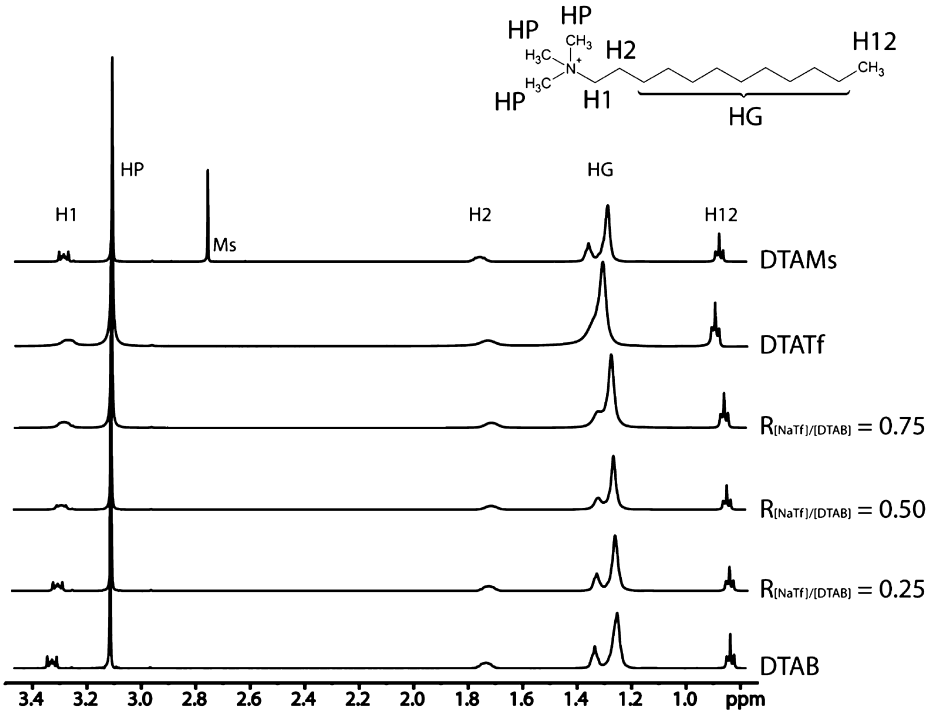

Figure 3. ^{1}H NMR spectra of 0.1 M DTAX for the pure and the different counterion:surfactant molar ratios ($R_{[NaTf]/[DTAB]}$). From top to bottom: DTAMs, DTATf, $R_{[NaTf]/[DTAB]}$ = 0.75, $R_{[NaTf]/[DTAB]}$ = 0.50, $R_{[NaTf]/[DTAB]}$ = 0.25, DTAB. Inset: Surfactant structure and proton nomenclature.

Table 3. Calculated Order Parameters (S) for Protons at Different Chain Positions in DTAX Micelles (X = Ms, Br, and Tf as counterions)[a]

DTAX	HP (headgroup)	HG (chain)	H12 (terminal CH_3)
Ms^-	0.04	0.28	0.12
Br^-	0.05	0.32	0.12
Tf^-	0.24	0.47	0.18

[a][DTAX] = 0.1 M.

DTAMs. This effect was great enough to lead to a more ordered HP than H12 in the DTATf case. The ordering effect extended through all the DTA hydrophobic chains. For the HG and H12 protons, S increased 1.5 times from DTAB or DTAMs to DTATf.

NOESY cross-peaks between H12 and the HP, H1, and H2 protons were observed in the DTAB aggregates with τ_{mix} exceeding 1 s and in DTATf with τ_{mix} exceeding 0.25 s. The NOE cross-peaks between H12 and HP, H1, and H2 in DTATf and DTAB can be explained by two effects: the folding of the

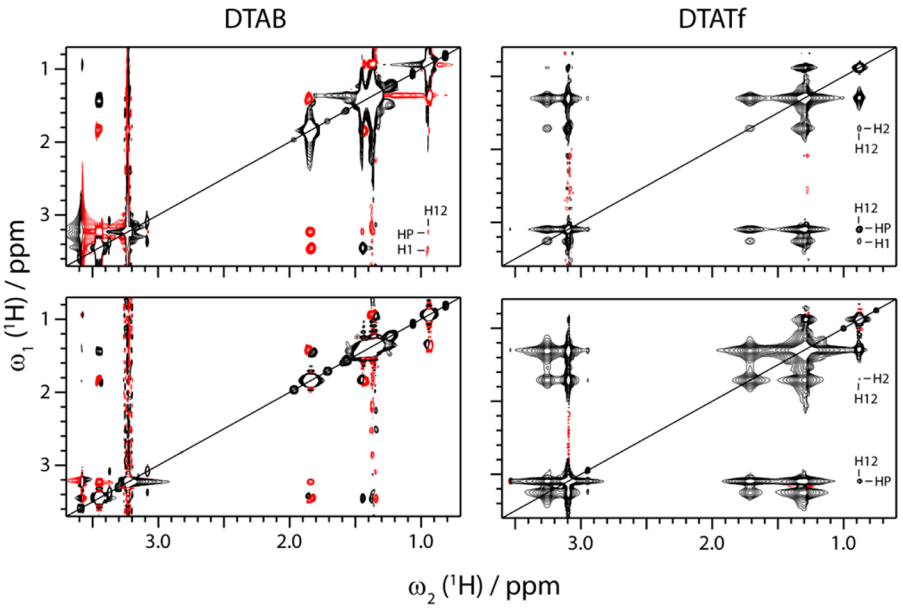

Figure 4. 2D ^{1}H–^{1}H NOE spectra of 0.3 M DTAB and 0.1 M DTATf recorded with mixing times of 1 s (top) or 0.2 s for DTAB and 0.25 s for DTATf (bottom): black, positive peaks; red, negative peaks.

dx.doi.org/10.1021/la304658e | Langmuir 2013, 29, 4193–4203

chains, which cause the end of the hydrophobic chain to be near the headgroup, or the proximity between the terminal $-CH_3$ in the DTA hydrophobic chain and the micellar interface, as in an interdigitated system. These effects may also occur simultaneously. These NOEs were absent or were at the noise level in the nonmicellized DTA^+ 2D NOE spectra acquired under the same mixing time, indicating that spin diffusion is not the major contribution to the NOE effect (Figure 5, Supporting Information). Consistent with the ordering effect of the triflate ion, the 2D NOE spectra of DTAB showed negative NOE cross-peaks. By contrast, positive cross-peaks were observed for DTATf, reflecting a more restricted mobility of the DTA chains in the DTATf aggregates (Figure 4).

Local Order, Dynamics, and Hydration in the DTAX Micelles. EPR. Spin labels have been widely used to obtain information on the structural and dynamic properties of the premicellar and micellar aggregates.[85−87] CAT16 and 5MESL probes were used to investigate interfacial properties of DTATf, DTAB, and DTAC micelles. In the CAT16 spin label, the nitroxide moiety is located at the headgroup of a hexadecyldimethylammonium molecule, whereas in 5MESL the nitroxide moiety is located at carbon 5 of stearic acid methyl ester. Despite the structural differences in the aggregates studied here, it seems to be reasonable to assume a similar position (on average) for the probes when incorporated into the different aggregates, based on the structure of CAT16 and the studies reported for 5MESL.[87]

For motionally narrowed EPR spectra, the difference in the rate of motion can be quantitatively estimated by calculating the rotational correlation times ($\tau_{measured}$). Figure 5 presents the

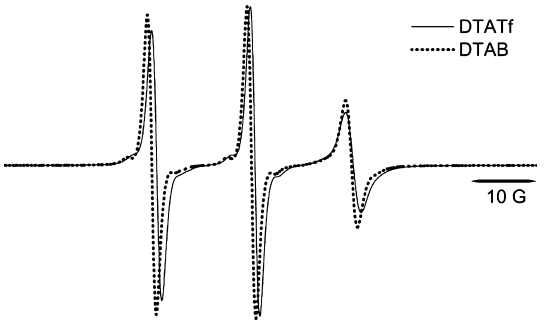

Figure 5. EPR spectra of the spin label 5MESL incorporated into DTATf and DTAB (both at 0.1 M) micelles.

EPR spectra of 5MESL incorporated into DTAB and DTATf micelles. All spectra in Figure 5 display narrow lines, indicating a fast tumbling of the probe on the EPR time scale. The incorporation of the probe into the DTATf aggregates led to a differential line broadening, as indicated by the high field line, which indicates a slower tumbling of the probe incorporated into the DTATf compared to the DTAB and DTAC micelles. In comparison to the DTAB and DTAC micelles (not shown), a similar slower tumbling was also observed for CAT16 incorporated into DTATf micelles. Because all EPR spectra displayed narrow lines, indicating a high degree of fast motion, the measured spectra were used to calculate the rotational correlation times, as described in the Methods section (Table 4). Compared with the values measured for the DTAB and DTAC micelles, τ_{probe} of the micellized CAT16 and 5MESL was clearly higher in DTATf. According to the Stokes−Einstein

Table 4. Rotational Correlation Time, τ_{probe}, and Hyperfine Coupling, a_N, of CAT16 and 5MESL in DTATf, DTAB, and DTAC Micelles

	CAT16		5MESL	
DTAX (M)	$\tau_{probe}/10^{-10}$ s	a_N/G	$\tau_{probe}/10^{-10}$ s	a_N/G
DTATf (0.1)	6.66	16.17	8.40	14.75
DTAB (0.1)	3.87	16.12	5.69	14.95
DTAC (0.08)	3.08	16.12	4.74	15.00

equation, rotational correlation times increase with increasing molecular size, increasing viscosity of the environment and decreasing temperature. Because we used the same spin label at the same temperature in these experiments, the higher values of τ_{probe} for the two probes in the DTATf micelles suggest a higher local viscosity at the interface of the DTATf micelles compared with the values for DTAB and DTAC, suggesting a higher packing of the molecules in the DTATf aggregates. The contribution of τ_s to $\tau_{measured}$ was approximately 6% in all cases.

The isotropic hyperfine splitting, a_N, measured in the EPR spectrum is polarity-dependent and decreases with a decrease in the polarity of the environment probed by the spin label. The values of a_N were determined from the separation between the low field and the center field lines. Table 4 presents the values of a_N for CAT16 and 5MESL incorporated into DTATX micelles. In the case of CAT16, a_N values were similar for all DTAX micelles, indicating an environment with similar polarity in all micelles, an expected result given the probe's structure. However, in the case of 5MESL, the values of a_N differed and were similar for DTAB and DTAC and lower for DTATf, indicating an environment with low polarity for DTATf due to the less hydrated interface in DTATf micelles.

Molecular Dynamics Modeling. Our MD simulations, as described in Methods, started with a bilayer arrangement with water-exposed edges. After ca. one nanosecond simulation time, the water exposure at the edges disappeared and a rim was formed (not shown).

The proximal distribution function and lifetime (τ_b) as a function of the distance from the micelle surface—taking r_{ul} as the coordinate—for triflate is shown in Figure 6. The values of

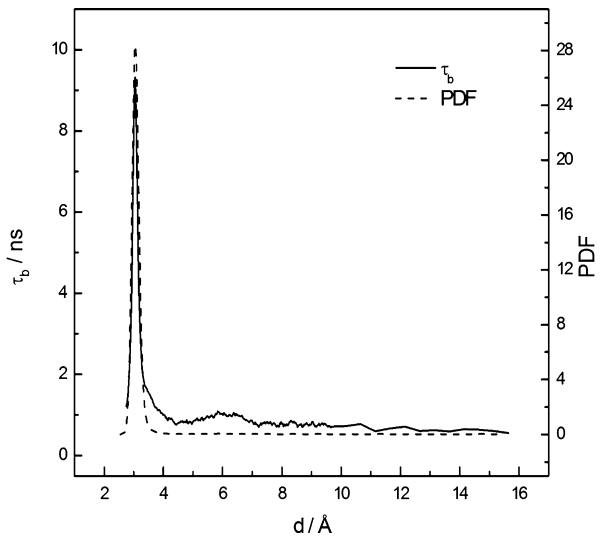

Figure 6. Lifetime of triflate (τ_b) and proximal distribution function (PDF) of the triflate center of mass as a function of the distance from the micelle surface.

dx.doi.org/10.1021/la304658e | Langmuir 2013, 29, 4193−4203

τ_b were calculated as described in the Methods section. The distance of a triflate COM to the closest object of the DTA^+ aggregate was analyzed from 2.8 Å to 16.0 Å in increments of 0.02 Å. To obtain detailed, reproducible, and statistically significant data, a fixed difference of 0.3 Å was imposed between r_{ul} and r_{ll}.

The proximal distribution function showed one distinct peak at 3 Å, while the window lifetime showed also the sharp peak near 3 Å and a smaller second peak around 6 Å (Figure 6). For longer distances (i.e., >8 Å) the τ_b and the distribution function functions were both constant, because triflate is freely diffusing in bulk solution. Defining bound ions as those residing at distances smaller than 4.6 Å, where the first peaks in both curves decayed (Figure 6), an ionization degree of 0.13 was obtained. If the second peak in the τ_b curve (Figure 6) is included, the ionization degree was 0.11. Both estimates of α were near the reported experimental value of 0.12,[13] demonstrating the capability of the used triflate ion force field to reproduce the experimental number.

Snapshots of the DTATf and DTAB aggregates taken at different times along the simulation are shown in Figure 7.

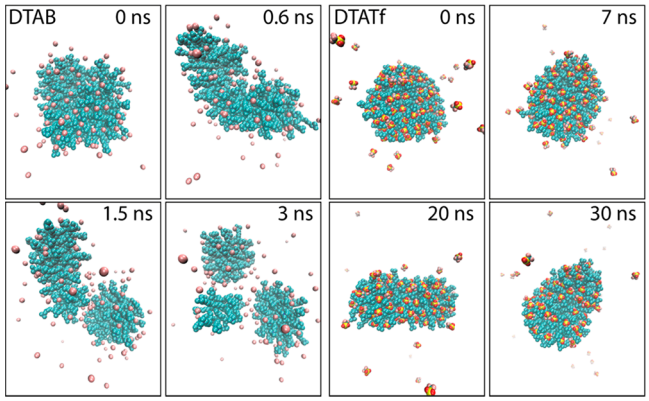

Figure 7. Snapshots of the DTAB and DTATf simulations with 130 monomers. The atom labeling is as follows: blue, C; dark blue, N; pink, Br^-; yellow, S; red, O; light pink, F. Water molecules were removed for clarity.

After only 0.3 ns, the DTAB micelle began to change from its initial oblate shape to a prolate object. A relatively high fraction of the Br^- atoms moved away from the DTA aggregate. After 1.4 ns, the aggregate became unstable, splitting the micelle into two aggregates, one with approximately 50 monomers and another with nearly 80 monomers. At 2 ns, another division occurred, yielding a smaller cluster of approximately 20 monomers and a larger micelle of almost 60 monomers. The Br^- atoms freely exchanged between the three aggregates. The DTATf aggregate exhibited a higher degree of stability in the oblate geometry than DTAB: at the beginning of the simulation, a high fraction of Tf^- moved to the DTA aggregate interface and the frequency of exit from the r_b to higher distances was small during the full simulation time. The aggregate maintained the initial shape over the first 7 ns, followed by a fluctuation of the micelle between an oblate and a prolate object.

Using higher aggregation numbers than the experimental values, the results obtained with the DTAB aggregate showed that a micelle under these conditions was very unstable, with a split observed even during the equilibrium time of the simulation. Due to the relatively low affinity of the bromide ion for the micelle interface, the headgroup repulsion of the DTA^+ monomers was too high to permit the packing of the DTA^+ monomers into a large aggregate. The energetically favorable aggregation had a nearly spherical symmetry with few monomers. The first step before the micellar splitting was a deformation of the initial disk-like shape to a rod-like structure, with fewer counterions bound to the aggregate. A further bending of the micelle led to a ring-like wrinkling state and, finally, to an aggregate cleavage. The exit rate of the counterion from DTAB aggregate interface was higher than it was for the DTATf simulation. The DTATf cluster with 130 monomers was stable, demonstrating that the triflate ion was capable of aggregating with the DTA^+ molecules at higher N_{agg} values than the bromide anions. Although shape fluctuations were observed during the simulation (Figure 7), no micellar cleavage was observed during the 35 ns of simulation.

General Discussion and Conclusions. The magnitude of the N_{agg} for DTATf can only be rationalized by nonspherical micelles. The SAXS best-fit shape function suggested a membrane-like model that cannot be infinite because we measured distinct sizes for the DTATf aggregate. The simplest model for these types of aggregates was a bicelle, i.e., a small planar bilayer fragment with rims. In addition to this unusual shape, the SAXS analysis suggested that the chains on opposite sides in the bilayer portion of the aggregate might be interdigitated.

With the addition of NaTf to DTAB, the mobility of the H atoms in the headgroup of DTA^+ was significantly affected. Low interfacial mobility of the triflate at the DTATf interface has been observed,[41] supporting a highly packed aggregate. The order parameters, calculated from the relaxation and overall tumbling times, showed that the packing at the DTATf interface was higher than that determined for DTAB or DTAMs. The interfacial ordering effect was transmitted through the DTA hydrocarbon chain to the terminal methyl group. Anions that insert into the interface of the surfactant monolayer induce an ordering in the surfactant chain.[88,89] Because Ms^- does not produce chain ordering, Tf^- through the dehydrated $-CF_3$ moiety must, to some extent, insert into the micellar core. This insertion would certainly favor a high stability of the electrostatically stabilized interaction of the sulfonate group with the trimethylammonium group.[13] Smaller distances between the terminal $-CH_3$ group and the protons HP, H1, and H2, which are necessarily near the interface,[90] in DTATf were indicated by the NOESY results. These NOEs could arise from a folding of the hydrophobic chain and/or from interdigitation. The model used to fit the SAXS results suggests that interdigitation is a distinct possibility.

In line with the NMR results, the EPR results revealed that the packing density of the DTATf aggregates was greater than that of the DTAC or DTAB aggregates. CAT16 seems to be exposed to a water-rich environment in the three surfactants. A lower hydration of the DTATf aggregates compared to the DTAC and DTAB aggregates was suggested by the 5MESL experiments, similar to the results from spectroscopic measurements.[41] The differences in the shape and hydration of the DTATf and DTAB or DTAC aggregates may be related to the properties of the surfactant-DNA gel particles prepared with these surfactants.[91]

Molecular dynamics confirmed both the high Tf^- affinity for the interface and the stability of the bicelle-like DTATf aggregate. In addition, our calculations showed that in silico,

dx.doi.org/10.1021/la304658e | Langmuir 2013, 29, 4193−4203

bromide cannot replace Tf^- in an object of similar shape and size.

■ ASSOCIATED CONTENT

Supporting Information

Intensity as a function of time plot from TRFQ of two [DTATf] samples in the presence of different quencher concentration; SAXS scattering curve of solid DTATf; SAXS curve obtained for aqueous DTATf at different concentrations; SAXS curves obtained for different [DTATf] in water and NaTf; T_1 and T_2 values for three DTAX 0.1 M samples; 2D $^1H-^1H$ NOE spectra of [DTAMs]; Source code for treating TRFQ data. This material is available free of charge via the Internet at http://pubs.acs.org.

■ AUTHOR INFORMATION

Corresponding Author

*E-mail: hchaimo@usp.br.

Author Contributions

F.S.L., I.M.C., and H.C. designed the experiments and wrote the paper. F.S.L. conducted the experiments and analysis. These authors specifically contributed to the following (methods): E.L.B. and A.C.B.R. (TRFQ); L.Q.A. and K.A.R. (SAXS); R.K.S., P.A.R.P., D.C.F. and O.A.E.S. (NMR); S.S. and J.C.B.Jr (EPR); D.H. (and L.G.D. for the initial calculations) (MD). All authors contributed to the final version of this manuscript.

Notes

The authors declare no competing financial interest.

■ ACKNOWLEDGMENTS

The authors are grateful to Francesco Spinozzi for allowing us to use the GENFIT program and for his help with the fitting procedure in the SAXS analysis. The financial support of FAPESP (Proc. No. 2007/50970-5), CNPq, Instituto Nacional de Ciência e Tecnologia de Fluidos Complexos (INCT-FCx) and Núcleo de Apoio à Pesquisa de Fluidos Complexos (NAP-FCx) are gratefully acknowledged. F.S.L. is a FAPESP graduate fellow (Proc. No. 2008/50041-7).

■ ABBREVIATIONS

DTA, Dodecyltrimethylammonium cation; Cl^-, Chloride; Br^-, Bromide; Ms^-, Methanesulfonate; Tf^-, Trifluoromethanesulfonate, triflate; α, Ionization degree; cmc, Critical micellar concentration; N_{agg}, Aggregation number; q^*, Position of the interference peak; d^*, Correlation distance of interaction peak; q_1, Position of large bilayer band; d_1, Bilayer total thickness ($2R_{shell} + 2R_{core}$); $\langle d \rangle$, Mean distance between aggregates; R_{shell}, Thickness of headgroup layer in DTATf aggregate; ρ_{shell}, Electron density of R_{shell}; R_{core}, Thickness of the hydrophobic core in DTATf aggregate; ρ_{core}, Electron density of R_{core}; T_1, Longitudinal magnetization relaxation time; T_2, Transverse magnetization relaxation time; S, Order parameter; τ_s, Tumbling time of the aggregate; CAT16, EPR probe; 5MESL, EPR probe; τ_{probe}, Rotational correlation time of EPR probe corrected by τ_s; a_N, Isotropic hyperfine splitting; τ_b, Lifetime of triflate as a function of distance from micelle surface; N_A, Avogadro constant; COM, Center of mass

■ REFERENCES

(1) Corrin, M. L.; Harkins, W. D. The Effect of Salts on the Critical Concentration for the Formation of Micelles in Colloidal Electrolytes. *J. Am. Chem. Soc.* **1947**, *69* (3), 683−688.

(2) Gamboa, C.; Sepúlveda, L. High viscosities of cationic and anionic micellar solutions in the presence of added salts. *J. Colloid Interface Sci.* **1986**, *113* (2), 566−576.

(3) Balmbra, R. R.; Clunie, J. S.; Goodman, J. F. Cubic Mesomorphic Phases. *Nature* **1969**, *222* (5199), 1159−&.

(4) Varade, D.; Aramaki, K.; Stubenrauch, C. Phase diagrams of water−alkyltrimethylammonium bromide systems. *Colloids Surf., A* **2008**, *315* (1−3), 205−209.

(5) Mehta, S. K.; Bhasin, K. K.; Chauhan, R.; Dham, S. Effect of temperature on critical micelle concentration and thermodynamic behavior of dodecyldimethylethylammonium bromide and dodecyltrimethylammonium chloride in aqueous media. *Colloids Surf., A: Physicochem. Eng. Aspects* **2005**, *255* (1−3), 153−157.

(6) Zielinski, R. Effect of temperature on micelle formation in aqueous NaBr solutions of octyltrimethylammonium bromide. *J. Colloid Interface Sci.* **2001**, *235* (2), 201−209.

(7) Mukerjee, P.; Mysels, K.; Kapauan, P. Counterion Specificity in the Formation of Ionic Micelles - Size, Hydration, and Hydrophobic Bonding Effects. *J. Phys. Chem.* **1967**, *71* (13), 4166−4175.

(8) Brady, J. E.; Evans, D. F.; Warr, G. G.; Grieser, F.; Ninham, B. W. Counterion Specificity as the Determinant of Surfactant Aggregation. *J. Phys. Chem.* **1986**, *90* (9), 1853−1859.

(9) Missel, P. J.; Mazer, N. A.; Carey, M. C.; Benedek, G. B. Influence of alkali-metal counterion identity on the sphere-to-rod transition in alkyl sulfate micelles. *J. Phys. Chem.* **1989**, *93* (26), 8354−8366.

(10) Cates, M. E.; Candau, S. J. Statics and dynamics of worm-like surfactant micelles. *J. Phys.: Condens. Matter* **1990**, *2* (33), 6869.

(11) Swanson-Vethamuthu, M.; Feitosa, E.; Brown, W. Salt-induced sphere-to-disk transition of octadecyltrimethylammonium bromide micelles. *Langmuir* **1998**, *14*, 1590−1596.

(12) Bales, B. L.; Zana, R. Cloud point of aqueous solutions of tetrabutylammonium dodecyl sulfate is a function of the concentration of counterions in the aqueous phase. *Langmuir* **2004**, *20* (5), 1579−1581.

(13) Lima, F. L., F. S.; Maximiano, F. A.; Cuccovia, I. M.; Chaimovich, H. Surface Activity of the Triflate Ion at the Air/Water Interface and Properties of N,N,N-Trimethyl-N-Dodecylammonium Triflate Aqueous Solutions. *Langmuir* **2011**, *27* (8), 4319−4323.

(14) Israelachvili, J. N.; Mitchell, D. J.; Ninham, B. W. Theory of self-assembly of hydrocarbon amphiphiles into micelles and bilayers. *J. Chem. Soc., Faraday Trans. 2* **1976**, *72*, 1525−1568.

(15) Tanford, C., *The hydrophobic effect: formation of micelles and biological membranes*; Wiley: New York, 1980.

(16) Evans, D. F.; Mitchell, D. J.; Ninham, B. W. Ion Binding and Dressed Micelles. *J. Phys. Chem.* **1984**, *88* (25), 6344−6348.

(17) Johnson, I.; Olofsson, G.; Jonsson, B. Micelle formation of ionic amphiphiles. Thermochemical test of a thermodyanamic model. *J. Chem. Soc., Faraday Trans. 2* **1987**, *83* (11), 3331−3344.

(18) Ruckenstein, E.; Beunen, J. A. Effect of counterion binding on micellization. *Langmuir* **1988**, *4* (1), 77−90.

(19) Puvvada, S.; Blankschtein, D. Thermodynamic description of micellization, phase behavior, and phase separation of aqueous solutions of surfactant mixtures. *J. Phys. Chem.* **1992**, *96* (13), 5567−5579.

(20) Boström, M.; Williams, D. R. M.; Ninham, B. W. Ion Specificity of Micelles Explained by Ionic Dispersion Forces. *Langmuir* **2002**, *18* (16), 6010−6014.

(21) Jusufi, A.; Hynninen, A.-P.; Haataja, M.; Panagiotopoulos, A. Z. Electrostatic Screening and Charge Correlation Effects in Micellization of Ionic Surfactants. *J. Phys. Chem. B* **2009**, *113* (18), 6314−6320.

(22) Hayter, J. B. A Self-Consistent Theory of Dressed Micelles. *Langmuir* **1992**, *8* (12), 2873−2876.

(23) Srinivasan, V.; Blankschtein, D. Effect of counterion binding on micellar solution behavior: 1. Molecular-thermodynamic theory of micellization of ionic surfactants. *Langmuir* **2003**, *19* (23), 9932−9945.

(24) Brown, W.; Johansson, K.; Almgren, M. Threadlike micelles from cetyltrimethylammonium bromide in aqueous sodium naphthalenesulfonate solutions studied by static and dynamic light scattering. *J. Phys. Chem.* **1989**, *93* (15), 5888−5894.

(25) Magid, L. J.; Han, Z.; Warr, G. G.; Cassidy, M. A.; Butler, P. D.; Hamilton, W. A. Effect of Counterion Competition on Micellar Growth Horizons for Cetyltrimethylammonium Micellar Surfaces: Electrostatics and Specific Binding. *J. Phys. Chem. B* **1997**, *101* (40), 7919−7927.
(26) Göbel, S.; Hiltrop, K., Influence of organic counterions on the structure of lyotropic mesophases. In *Trends in Colloid and Interface Science V*, Corti, M.; Mallamace, F., Eds.; Springer: Berlin/Heidelberg, 1991; Vol. *84*, pp 241−242.
(27) Lin, Z.; Cai, J. J.; Scriven, L. E.; Davis, H. T. Spherical-to-Wormlike Micelle Transition in CTAB Solutions. *J. Phys. Chem.* **1994**, *98* (23), 5984−5993.
(28) Tapia, M. J.; Burrows, H. D.; Azenha, M. E. D. G.; Miguel, M. D.; Pais, A. A. C. C.; Sarraguca, J. M. G. Cation association with sodium dodecyl sulfate micelles as seen by lanthanide luminescence. *J. Phys. Chem. B* **2002**, *106* (27), 6966−6972.
(29) Harada, M.; Satou, H.; Okada, T. Hydration structures of bromides on cationic micelles. *J. Phys. Chem. B* **2007**, *111* (42), 12136−12140.
(30) Geng, Y.; Romsted, L. S.; Froehner, S.; Zanette, D.; Magid, L. J.; Cuccovia, I. M.; Chaimovich, H. Origin of the Sphere-to-Rod Transition in Cationic Micelles with Aromatic Counterions: Specific Ion Hydration in the Interfacial Region Matters. *Langmuir* **2005**, *21* (2), 562−568.
(31) Cuccovia, I. M.; Agostinho-Neto, A.; Wendel, C. M. A.; Chaimovich, H.; Romsted, L. S. Determination of Interfacial Co-ion Concentration in Ionic Micelles by Chemical Trapping: Halide Concentration at the Interface of Sodium Dodecyl Sulfate Micelles. *Langmuir* **1997**, *13* (19), 5032−5035.
(32) Romsted, L. S. Do Amphiphile Aggregate Morphologies and Interfacial Compositions Depend Primarily on Interfacial Hydration and Ion-Specific Interactions? The Evidence from Chemical Trapping. *Langmuir* **2006**, *23* (2), 414−424.
(33) Talens-Alesson, F. The Role of Ionic Pair Association on Micellization and Counterion Binding in Ionic Micelles. *J. Phys. Chem. B* **2009**, *113* (29), 9779−9785.
(34) Moreira, L.; Firoozabadi, A. Molecular Thermodynamic Modeling of Specific Ion Effects on Micellization of Ionic Surfactants. *Langmuir* **2010**, *26* (19), 15177−15191.
(35) Marcus, Y. Surface Tension of Aqueous Electrolytes and Ions. *J. Chem. Eng. Data* **2010**, *55* (9), 3641−3644.
(36) Barry, B. W.; Wilson, R. CMC Counterion Binding and Thermodynamics of Ethoxylated Anionic and Cationic Surfactants. *Colloid Polym. Sci.* **1978**, *256* (3), 251−260.
(37) Perger, T. M.; Bester-Rogac, M. Thermodynamics of micelle formation of alkyltrimethylammonium chlorides from high performance electric conductivity measurements. *J. Colloid Interface Sci.* **2007**, *313* (1), 288−295.
(38) Leontidis, E. Hofmeister anion effects on surfactant self-assembly and the formation of mesoporous solids. *Curr. Opin. Colloid Interface Sci.* **2002**, *7* (1−2), 81−91.
(39) Bergstrom, P. A.; Lindgren, J. An Infrared Spectroscopic Study of the Hydration of the Triflate Ion (Cf3so3-) in Aqueous-Solution. *J. Mol. Struct.* **1990**, *239*, 103−111.
(40) Cione, A. M.; Mazyar, O. A.; Booth, B. D.; McCabe, C.; Jennings, G. K. Deposition and Wettability of [bmim][triflate] on Self-Assembled Monolayers. *J. Phys. Chem. C* **2009**, *113* (6), 2384−2392.
(41) Submitted for publication.
(42) Infelta, P. P.; Gratzel, M.; Thomas, J. K. Luminescence Decay of Hydrophobic Molecules Solubilized in Aqueous Micellar Systems - Kinetic-Model. *J. Phys. Chem.* **1974**, *78* (2), 190−195.
(43) Tachiya, M. Application of a Generating Function to Reaction-Kinetics in Micelles - Kinetics of Quenching of Luminescent Probes in Micelles. *Chem. Phys. Lett.* **1975**, *33* (2), 289−292.
(44) Alargova, R. G.; Kochijashky, I. I.; Sierra, M. L.; Zana, R. Micelle aggregation numbers of surfactants in aqueous solutions: A comparison between the results from steady-state and time-resolved fluorescence quenching. *Langmuir* **1998**, *14* (19), 5412−5418.
(45) Spinozzi, F. http://www.isf.univpm.it/biophysics/software.htm.
(46) Mariani, P.; Spinozzi, F.; Federiconi, F.; Amenitsch, H.; Spindler, L.; Drevensek-Olenik, I. Small Angle X-ray Scattering Analysis of Deoxyguanosine 5 ′-Monophosphate Self-Assembing in Solution: Nucleation and Growth of G-Quadruplexes. *J. Phys. Chem. B* **2009**, *113* (22), 7934−7944.
(47) Villeneuve, M.; Ootsu, R.; Ishiwata, M.; Nakahara, H. Research on the vesicle-micelle transition by H-1 NMR relaxation measurement. *J. Phys. Chem. B* **2006**, *110* (36), 17830−17839.
(48) Wennerstrom, H.; Lindman, B.; Soderman, O.; Drakenberg, T.; Rosenholm, J. B. C-13 Magnetic-Relaxation in Micellar Solutions - Influence of Aggregate Motion on T1. *J. Am. Chem. Soc.* **1979**, *101* (23), 6860−6864.
(49) Nery, H.; Soderman, O.; Canet, D.; Walderhaug, H.; Lindman, B. Surfactant Dynamics in Spherical and Nonspherical Micelles - a Nuclear-Magnetic-Resonance Study. *J. Phys. Chem.* **1986**, *90* (22), 5802−5808.
(50) Wasylishen, R. E.; Kwak, J. C. T.; Gao, Z. S.; Verpoorte, E.; Macdonald, J. B.; Dickson, R. M. Nmr-Studies of Hydrocarbons Solubilized in Aqueous Micellar Solutions. *Can. J. Chem.* **1991**, *69* (5), 822−833.
(51) Ortega, A.; de la Torre, J. G. Hydrodynamic properties of rodlike and disklike particles in dilute solution. *J. Chem. Phys.* **2003**, *119* (18), 9914−9919.
(52) Barr, D.; Jiang, J. J.; Weber, R. T. How to quantitate nitroxide spin adduct using TEMPOL; *Bruker Manual - Experimental Techniques*, 1996; Note 3.
(53) Kivelson, D. Theory of Esr Linewidths of Free Radicals. *J. Chem. Phys.* **1960**, *33* (4), 1094−1106.
(54) Freed, J. H.; Fraenkel, G. K. Theory of Linewidths in Electron Spin Resonance Spectra. *J. Chem. Phys.* **1963**, *39* (2), 326−&.
(55) Schreier, S.; Polnaszek, C. F.; Smith, I. C. P. Spin Labels in Membranes Problems in Practice. *Biochim. Biophys. Acta* **1978**, *515* (4), 375−436.
(56) Bales, B. L.; Zana, R. Characterization of micelles of quaternary ammonium surfactants, as reaction media I: Dodeclytrimethylammonium bromide and chloride. *J. Phys. Chem. B* **2002**, *106* (8), 1926−1939.
(57) Wikander, G.; Johansson, L. B. A. Micelle Size Determined by Electron-Spin Resonance and Fluorescence Spectroscopy. *Langmuir* **1989**, *5* (3), 728−733.
(58) Martínez, L.; Andrade, R.; Birgin, E. G.; Martínez, J. M. PACKMOL: a package for building initial configurations for molecular dynamics simulations. *J. Comput. Chem.* **2009**, *30* (13), 2157−2164.
(59) Jorgensen, W. L.; Maxwell, D. S.; Tirado-Rives, J. Development and testing of the OPLS all-atom force field on conformational energetics and properties of organic liquids. *J. Am. Chem. Soc.* **1996**, *118* (45), 11225−11236.
(60) Canongia Lopes, J. N.; Pádua, A. A. H. Molecular Force Field for Ionic Liquids Composed of Triflate or Bistriflylimide Anions. *J. Phys. Chem. B* **2004**, *108* (43), 16893−16898.
(61) Horinek, D.; Herz, A.; Vrbka, L.; Sedlmeier, F.; Mamatkulov, S. I.; Netz, R. R. Specific ion adsorption at the air/water interface: The role of hydrophobic solvation. *Chem. Phys. Lett.* **2009**, *479* (4−6), 173−183.
(62) Pal, S.; Bagchi, B.; Balasubramanian, S. Hydration layer of a cationic micelle, C(10)TAB: Structure, rigidity, slow reorientation, hydrogen bond lifetime, and solvation dynamics. *J. Phys. Chem. B* **2005**, *109* (26), 12879−12890.
(63) Shang, B. Z.; Wang, Z. W.; Larson, R. G. Effect of Headgroup Size, Charge, and Solvent Structure on Polymer-Micelle Interactions, Studied by Molecular Dynamics Simulations. *J. Phys. Chem. B* **2009**, *113* (46), 15170−15180.
(64) Hess, B.; Kutzner, C.; van der Spoel, D.; Lindahl, E. GROMACS 4: Algorithms for Highly Efficient, Load-Balanced, and Scalable Molecular Simulation. *J. Chem. Theory Comput.* **2008**, *4* (3), 435−447.
(65) Tehrani-Bagha, A. R.; Kärnbratt, J.; Löfroth, J. E.; Holmberg, K. Cationic ester-containing gemini surfactants: Determination of aggregation numbers by time-resolved fluorescence quenching. *J. Colloid Interface Sci.* **2012**, *376* (1), 126−132.

(66) Aswal, V. K.; Goyal, P. S. Role of different counterions and size of micelle in concentration dependence micellar structure of ionic surfactants. *Chem. Phys. Lett.* **2003**, *368* (1−2), 59−65.
(67) Ozeki, S.; Ikeda, S. The Sphere Rod Transition of Micelles and the 2 Step Micellization of Dodecyltrimethylammonium Bromide in Aqueous Nabr Solutions. *J. Colloid Interface Sci.* **1982**, *87* (2), 424−435.
(68) Malliaris, A.; Lemoigne, J.; Sturm, J.; Zana, R. Temperature-Dependence of the Micelle Aggregation Number and Rate of Intramicellar Excimer Formation in Aqueous Surfactant Solutions. *J. Phys. Chem.* **1985**, *89* (12), 2709−2713.
(69) Mata, J.; Varade, D.; Bahadur, P. Aggregation behavior of quaternary salt based cationic surfactants. *Thermochim. Acta* **2005**, *428* (1−2), 147−155.
(70) Ozeki, S.; Ikeda, S. The Stability of Spherical Micelles of Dodecyltrimethylammonium Chloride in Aqueous Nacl Solutions. *Bull. Chem. Soc. Jpn.* **1981**, *54* (2), 552−555.
(71) Roelants, E.; Deschryver, F. C. Parameters Affecting Aqueous Micelles of Ctac, Ttac, and Dtac Probed by Fluorescence Quenching. *Langmuir* **1987**, *3* (2), 209−214.
(72) Griffiths, P. C.; Paul, A.; Heenan, R. K.; Penfold, J.; Ranganathan, R.; Bales, B. L. Role of counterion concentration in determining micelle aggregation: Evaluation of the combination of constraints from small-angle neutron scattering, electron paramagnetic resonance, and time-resolved fluorescence quenching. *J. Phys. Chem. B* **2004**, *108* (12), 3810−3816.
(73) Prevost, S.; Wattebled, L.; Laschewsky, A.; Gradzielski, M. Formation of Monodisperse Charged Vesicles in Mixtures of Cationic Gemini Surfactants and Anionic SDS. *Langmuir* **2011**, *27* (2), 582−591.
(74) Jackson, A. J.; Li, Z. X.; Thomas, R. K.; Penfold, J. The structures of micelles of alkytrimethylammonium perfluorocarboxylates and of their adsorbed layers at the air/water interface. *Phys. Chem. Chem. Phys.* **2002**, *4* (13), 3022−3031.
(75) Bergstrom, M.; Skov Pedersen, J. Structure of pure SDS and DTAB micelles in brine determined by small-angle neutron scattering (SANS). *Phys. Chem. Chem. Phys.* **1999**, *1* (18), 4437−4446.
(76) Bergstrom, M.; Pedersen, J. S. A small-angle neutron scattering (SANS) study of tablet-shaped and ribbonlike micelles formed from mixtures of an anionic and a cationic surfactant. *J. Phys. Chem. B* **1999**, *103* (40), 8502−8513.
(77) Taddei, G.; Amaral, L. Q. Bending energy and relative stability of micellar forms. *J. Phys. Chem.* **1992**, *96* (14), 6102−6104.
(78) Srinivasan, V.; Blankschtein, D. Prediction of conformational characteristics and micellar solution properties of fluorocarbon surfactants. *Langmuir* **2005**, *21* (4), 1647−1660.
(79) Belmajdoub, A.; Brondeau, J.; Boubel, J. C.; Canet, D. Slow Motions Undergone by Surfactant Molecules in Micelles - a H-1 and N-14 Nuclear Magnetic-Relaxation Study. *Chem. Phys. Lett.* **1987**, *140* (4), 389−393.
(80) Nusselder, J. J. H.; Engberts, J. B. F. N. A H-1-Nmr Study of the Order and Alkyl Chain Packing in the Core of Spherical Micelles Formed from 1-Methyl-4-Alkylpyridinium Iodide Surfactants. *J. Phys. Chem.* **1989**, *93* (16), 6142−6145.
(81) Bratt, P. J.; Gillies, D. G.; Sutcliffe, L. H.; Williams, A. J. Nmr Relaxation Studies of Internal Motions - a Comparison between Micelles and Related Systems. *J. Phys. Chem.* **1990**, *94* (7), 2727−2729.
(82) Zhao, S.; Yuan, H. Z.; Yu, J. Y.; Du, Y. R. Hydrocarbon chain packing in the micellar core of surfactants studied by H-1 NMR relaxation. *Colloid Polym. Sci.* **1998**, *276* (12), 1125−1130.
(83) Yang, Q. Q.; Zhou, Q.; Somasundaran, P. NMR study of micellar microstructures of cationic single-chain and gemini surfactants and their mixtures with nonionic surfactant n-dodecyl-beta-D-maltoside. *Colloids Surf., A: Physicochem. Eng. Aspects* **2008**, *322* (1−3), 40−46.
(84) Onoda-Yamamuro, N.; Yamamuro, O.; Tanaka, N.; Nomura, H. NMR and neutron scattering studies on spherical and rod-like micelles of dodecyltrimethylammonium bromide in aqueous sodium salicylate solutions. *J. Mol. Liq.* **2005**, *117* (1−3), 139−145.
(85) Ernandes, J. R.; Chaimovich, H.; Schreier, S. Spin Label Study of Detergents in Region of Critical Micelle Concentration. *Chem. Phys. Lipids* **1977**, *18* (3−4), 304−315.
(86) Ernandes, J. R.; Schreier, S.; Chaimovich, H. Spin Label Studies of Micellar and Pre-Micellar Aggregates. *Chem. Phys. Lipids* **1976**, *16* (1), 19−30.
(87) Lebedeva, N.; Bales, B. L. Location of spectroscopic probes in self-aggregating assemblies. I. The case for 5-doxylstearic acid methyl ester serving as a benchmark spectroscopic probe to study micelles. *J. Phys. Chem. B* **2006**, *110* (20), 9791−9799.
(88) Aroti, A.; Leontidis, E.; Maltseva, E.; Brezesinski, G. Effects of Hofmeister anions on DPPC Langmuir monolayers at the air-water interface. *J. Phys. Chem. B* **2004**, *108* (39), 15238−15245.
(89) Gurau, M. C.; Lim, S. M.; Castellana, E. T.; Albertorio, F.; Kataoka, S.; Cremer, P. S. On the mechanism of the Hofmeister effect. *J. Am. Chem. Soc.* **2004**, *126* (34), 10522−10523.
(90) Evans, D. F.; Wennerström, H. *The Colloidal Domain*, 2nd ed.; Wiley-VCH: Weinheim, 1999.
(91) Moran, M. C.; Alonso, T.; Lima, F. S.; Vinardell, M. P.; Miguel, M. G.; Lindman, B. Counter-ion effect on surfactant-DNA gel particles as controlled DNA delivery systems. *Soft Matter* **2012**, *8* (11), 3200−3211.